



Structural Failure of a Small Cargo Vessel Among Rough Seas

Y. Yamamoto and H. Ohtsubo, University of Tokyo, Tokyo, Japan
Y. Takeda, Ishikawajima-Harima Heavy Industries Co. Ltd., Tokyo, Japan
T. Fukasawa, University of Tsukuba, Ibaragi, Japan

ABSTRACT

A small cargo vessel of 48 m suffered from serious damages among rough seas, and its main hull was bent at S.S. 7 by a hogging moment. The ship under consideration was in ballast condition, and was carrying a large amount of ballast water in the fore peak tank. In this paper, the analysis based on hydroelasticity shows that this damage is caused by a hogging moment due to bottom slamming, although in the case of conventional ships slamming causes a large sagging moment in the mid-part. Elastic responses are calculated step-by-step for the ship idealized as a Timoshenko beam taking account of slamming impact forces determined with respect to instantaneous configurations. It is shown that slamming responses give hogging moment sufficient for the damage in an unlucky condition of waves corresponding to the sea state reported. Moreover, the collapsing strength of the ship is estimated with the aid of structural experiments.

INTRODUCTION

A small cargo ship in ballast condition suffered from serious damages among rough seas; its fore-body snapped off at S.S. 7, forming a plastic hinge there instantaneously. It is reported that she failed after passing through a pair of wave crests of 4 meters in height in seas of state 6. The damages were evidently caused by high hogging moment. Although in a conventional ship slamming causes large sagging moment in the middle part of the ship's hull [1, 2]*, the report suggests that slamming may play an important role for this problem. In the case of a small cargo ship in ballast condition, the ballast water is concentrated in the fore- and aft-peak tanks because of her single-bottom structure, and this causes large hogging moment in her middle part when in the still water condition. In general, lit-

tle attention has been paid to the fore-draft, and she may have had a large trim angle. It is a well-known fact that she may often encounter relatively high waves. She may frequently suffer, therefore, from bottom slamming in the middle part in actual sea conditions. This consideration can be confirmed by a report telling that bottom corrugations occur due to slamming pressure over a wide range of more than one-half of her length [3]. This fact suggests a possibility of occurrence of high hogging moment due to slamming in addition to the large still-water bending moment.

In this paper, the authors analyze the damage of the above-mentioned ship from the viewpoint of slamming. Her behavior in head seas moving into a wave train is investigated by idealizing her as an assemblage of the Timoshenko beam elements. Hydrodynamic impact on the bottom is closely related to her instantaneous wave-hull configurations, and therefore, calculations are performed by the step-by-step method. Histories of bending moment are compared with the ultimate collapsing moment which has been estimated with the help of structural experiments.

THEORY OF SHIP'S BEHAVIOR AMONG WAVES

Most previous authors have investigated the longitudinal bending moment in a ship among waves by the two-step approach; that is, its rigid body motion is calculated first by the conventional method, and then hull vibration responses are obtained by making use of the impact force estimated from the ship's relative velocity with respect to waves [4-8]. In reality, however, the ship's motion is influenced by the slamming impact, and this two-step approach may give unrealistic results. Meyerhoff and Schlachter [9] developed a nonlinear theory of a ship's motion among waves taking account of slamming impact, and determined the bending moment by the two-step approach.

Yamamoto, Fujino, and Fukasawa developed a nonlinear theory of a ship's

* Note: Numbers in brackets denotes references located on page

behavior among waves, assuming the ship to be an elastic beam. They applied Galerkin's method with the use of the lower harmonics, as has been successful for the analysis of large tanker-type ships and container carriers. In the case of small cargo vessels, however, higher harmonics may become of importance because the large slamming impacts act near the nodal points of lower vibration modes. For determining dynamic responses, the finite element method can be conveniently applied, and in the present paper, it is formulated by idealizing the ship's hull as a Timoshenko beam.

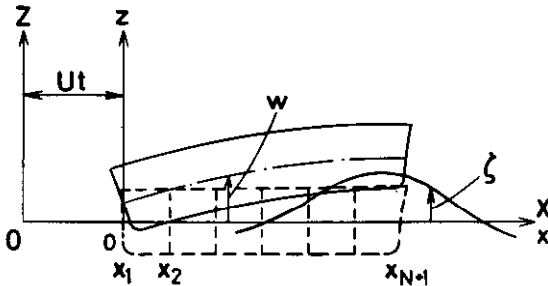


Fig. 1 Reference systems

The rectangular coordinate system (X, Y, Z) is introduced so that the X, Y-plane lies on the still water surface, and the Z-axis directs upward as shown in Fig. 1. Consider a ship advancing with a constant speed, U, in the positive X-direction. Introduce the moving coordinate system (x, y, z) moving with the ship so that the x, y-plane lies in the X, Y-plane keeping the x-axis parallel to the X-axis. Since the inclination of the ship girder is sufficiently small, the x-axis can be regarded as the element axis. Assume that a wave train travels in the negative X-direction.

Deformations of the ship's hull can be described by the upward total displacement, w, and the shear deflection, ws. The equation of motion of the ship's hull can be formulated as an elastic beam taking account of shear deformation, and disregarding the rotary inertia. It is given by

$$\frac{\partial}{\partial x} [GA_w (\frac{\partial w_s}{\partial x} + \eta_s \frac{\partial^2 w_s}{\partial t \partial x})] + f_z = m \frac{\partial^2 w}{\partial t^2} \quad (1)$$

$$\frac{\partial}{\partial x} [EI \frac{\partial}{\partial x} (\frac{\partial (w-w_s)}{\partial x} + \eta_b \frac{\partial^2 (w-w_s)}{\partial t \partial x})] + GA_w (\frac{\partial w_s}{\partial x} + \eta_s \frac{\partial^2 w_s}{\partial t \partial x}) = 0 \quad (2)$$

where m, EI, GA_w, η_b, η_s, and f_z are the mass per unit length, the flexural rigidity, the shear rigidity, the struc-

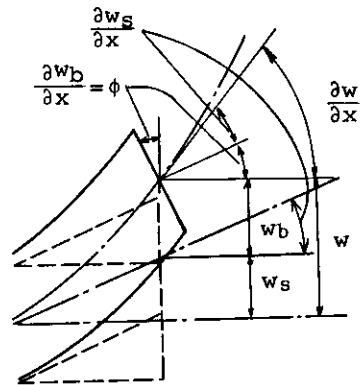


Fig. 2 Deformations of ship girder

tural damping coefficients for bending and shearing, and the external force, defined at each section of the ship. Here

$$w - w_s = w_b$$

is the flexural deflection.

On the same concept as the conventional strip method, the external force caused by the momentum change of fluid, f_m, is given by

$$f_m = - \frac{D}{Dt} [M_H (\frac{Dw}{Dt} - v_z)], \quad (3)$$

where M_H and v_z are the time-varying sectional added mass for vertical motion and the vertical component of the orbital velocity of the incident wave surface, and

$$\frac{D}{Dt} = \frac{\partial}{\partial t} - U \frac{\partial}{\partial x}. \quad (4)$$

The most significant term in the expression for f_m given by (3) is the impact force

$$f_{imp} = - \frac{\partial M_H}{\partial t} (\frac{Dw}{Dt} - v_z), \quad (5)$$

which is in proportion to the square of the relative velocity of the ship to the wave surface [10-12]. The damping force, f_r, due to wave-making, is in proportion to the relative velocity, and is given by

$$f_r = - N_H (\frac{Dw}{Dt} - v_z), \quad (6)$$

where N_H is the time-varying sectional wave-making damping coefficient for vertical motion.

Consider the pressure force, f_p. From Bernoulli's equation, the pressure, p, is given in the following form by disregarding terms of higher order:

$$p = -\rho \frac{D\phi}{Dt} - \rho g(z_0 + w), \quad (7)$$

where ϕ , ρ , g , and z_0 are the velocity potential of the incident wave train, the mass density of water, acceleration due to gravity, and the z -coordinate of a point on the hull in the still water condition (see Fig. 3). The pressure force is obtained by integrating it over the instantaneous wetted surface, C , of the hull; that is,

$$f_p = \int_C (-p) n_z ds, \quad (8)$$

where n_z is the z -component of the outward unit normal vector on the ship's surface in a transverse section. Introducing Eq. (7) into Eq. (8) leads to

$$\begin{aligned} f_p &= -\rho g \int_{-\bar{y}}^{\bar{y}} (z_0 + w - \zeta_w) dy \\ &= \rho g A. \end{aligned} \quad (9)$$

where A and ζ_w are the effective sectional area and the elevation of subsurface corresponding to the draft or the effective wave elevation given by

$$\zeta_w = \frac{1}{g} \frac{D\phi}{Dt}. \quad (10)$$

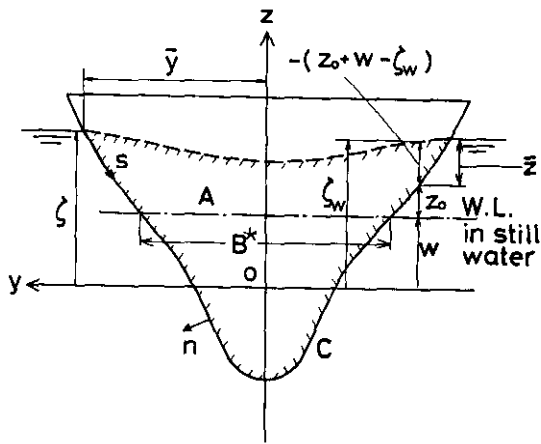


Fig. 3 Ship section and wave surface

Since the weight per unit length of the ship is given by

$$f_g = mg, \quad (11)$$

the total external force per unit length, f_z , is obtained by summing up all the components of the force;

$$f_z = f_m + f_r + f_p + f_g. \quad (12)$$

The displacement, w , can conveniently be divided into two parts, the linear

or rigid-body-motion mode and the vibration mode;

$$w = w_r + w_v. \quad (13)$$

The rigid-body-motion mode, w_r , can be expressed by

$$w_r = z_{\theta} + (x - \frac{L}{2}) \theta, \quad (14)$$

where z_{θ} and θ indicate heave and pitch. Actual heave and pitch motions are accompanied by some vibration mode. The vibration mode, w_v , is expressed as a sum of the flexural part, w_{vb} , and the shear deflection, w_s ;

$$w_v = w_{vb} + w_s, \quad (15)$$

where

$$w_{vb} = w_b - w_r.$$

The degrees of freedom corresponding to all the displacements, w , w_r , and w_s , have three redundancies; one is for giving a zero base of the shear deflection, and the other two are for the definition of the rigid-body-motion mode; therefore, it will be assumed that

$$\left. \begin{aligned} w_s &= 0 & \text{at } P_1, \\ w_v &= 0 & \text{at } P_1 \text{ and } P_2, \end{aligned} \right\} \quad (16)$$

where P_1 and P_2 are conveniently taken near the nodes of the ship's two-node vibration mode in still water [13].

For the sake of simplicity, it will be assumed that the structural damping can be expressed by the equivalent logarithmic decrement, δ_v , for each vibration mode such that [cf. Ref. 14]

$$\delta_r = 0, \quad (17)$$

$$\delta_v = \delta_2 \left(\frac{\omega_v}{\omega_2} \right) \quad \text{or} \quad \eta_b = \eta_s = \frac{\delta_2}{\pi \omega_2} \quad (18)$$

In the following example calculations, $\delta_2 = 0.056$ will be used [15].

The numerical procedure for solving (1) and (2) is based on the finite element analysis by discretizing the ship girder for the Timoshenko beam element at the nodal points, x_j , ($j = 1, \dots, N+1$; $x_{N+1} - x_1 = L$) (see Fig. 4). Assume that the displacement components, w_{vj} ($= w_v - w_s$) and w_{sj} , are given by cubic or linear polynomials in each element, respectively; they are expressed in terms of the nodal displacements, $(w_{vj} - w_{sj}, \theta_{bj})$ or w_{sj} , ($j = 1, \dots, N+1$), where

$$\theta_{bj} = \phi_j - \theta \quad (19)$$

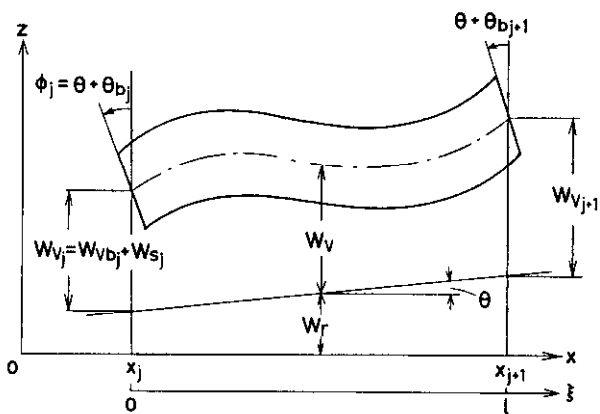


Fig. 4 Timoshenko beam idealization

The finite element formulation can be derived from Hamilton's Principle

$$\int_{t_1}^{t_2} [\delta(T - V) - \delta D + \delta W] dt = 0, \quad (20)$$

where the kinetic energy, T , the strain energy, V , the dissipation function, D , and the virtual work done by external force, δW , are such that

$$T = \frac{1}{2} \int_0^L m \left(\frac{\partial w}{\partial t} \right)^2 dx, \quad (21)$$

$$V[w, w_s] = \frac{1}{2} \int_0^L [EI \left(\frac{\partial^2 (w - w_s)}{\partial x^2} \right)^2 + GA_w \left(\frac{\partial w_s}{\partial x} \right)^2] dx, \quad (22)$$

$$\delta D = \eta_b \delta V|_{w=\dot{w}, w_s=\dot{w}_s}, \quad (23)$$

$$\delta W = \int_0^L f_z \delta w dx. \quad (24)$$

Let q_r and q_v be the totality of the degrees of freedom corresponding to the rigid-body-motion or vibration mode, respectively. Then the equation of motion derived from (20) is given in the following matrix form (see Appendix 1):

$$\begin{bmatrix} M_{rr} & M_{rv} \\ M_{vr} & M_{vv} \end{bmatrix} \begin{Bmatrix} \ddot{q}_r \\ \ddot{q}_v \end{Bmatrix} + \begin{bmatrix} 0 & 0 \\ 0 & C_{vv} \end{bmatrix} \begin{Bmatrix} \dot{q}_r \\ \dot{q}_v \end{Bmatrix} + \begin{bmatrix} 0 & 0 \\ 0 & K_{vv} \end{bmatrix} \begin{Bmatrix} q_r \\ q_v \end{Bmatrix} = \begin{Bmatrix} f_r \\ f_v \end{Bmatrix}. \quad (25)$$

This equation can be rewritten in the following form by expressing the hydrodynamical forces explicitly, which make numerical computations stable:

$$\begin{bmatrix} M_{rr} + M^*_{rr} & M_{rv} + M^*_{rv} \\ M_{vr} + M^*_{vr} & M_{vv} + M^*_{vv} \end{bmatrix} \begin{Bmatrix} \ddot{q}_r \\ \ddot{q}_v \end{Bmatrix} + \begin{bmatrix} C^*_{rr} & C^*_{rv} \\ C^*_{vr} & C_{vv} + C^*_{vv} \end{bmatrix} \begin{Bmatrix} \dot{q}_r \\ \dot{q}_v \end{Bmatrix} + \begin{bmatrix} K^*_{rr} & K^*_{rv} \\ K^*_{vr} & K_{vv} + K^*_{vv} \end{bmatrix} \begin{Bmatrix} q_r \\ q_v \end{Bmatrix} = \begin{Bmatrix} f^*_{r} \\ f^*_{v} \end{Bmatrix}, \quad (26)$$

where $[M^*_{rr} \ M^*_{rv}, M^*_{vr} \ M^*_{vv}]$, $[C^*_{rr} \ C^*_{rv}; C^*_{vr} \ C^*_{vv}]$, and $[K^*_{rr} \ K^*_{rv}, K^*_{vr} \ K^*_{vv}]$ are due to the added water mass, the wave-making damping force, and the buoyant force, respectively.

The equation of motion given by (26) will be integrated by the direct integration procedure, taking account of the nonlinear effects, and for this purpose, a Newmark beta method with $\beta = 1/4$ will be adopted from the viewpoint of stability and accuracy. Nonlinearities of the present problem arise from the underwater geometry of the ship and the impact force due to slamming; since the former is self-explanatory, the latter will be discussed in detail hereafter.

For estimating the hydrodynamic impact force, the time derivative of the added mass in (5) will be evaluated by the following formula:

$$\frac{\partial M_H}{\partial t} = \begin{cases} \frac{M_H}{\Delta t} \frac{\partial \bar{z}}{\partial t} & \text{for bottom impact,} \\ \frac{\partial M_H}{\partial z} \frac{\partial \bar{z}}{\partial t} & \text{otherwise,} \end{cases} \quad (27)$$

where \bar{z} and Δt are the instantaneous draft and a discrete time interval used for time integration. Because of its smallness, the hydrodynamic impact force can be disregarded when the ship section emerges from water; namely,

$$f_{\text{imp}} = \begin{cases} -\frac{\partial M_H}{\partial t} \left(\frac{Dw}{Dt} - v_z \right) & \text{if } \frac{Dw}{Dt} - v_z < 0, \\ 0 & \text{if } \frac{Dw}{Dt} - v_z \geq 0. \end{cases} \quad (28)$$

The validity of this assumption is confirmed by the results of the forced oscillation test shown in Fig. 5 [11]. Although they depend upon the encounter frequency, ω_e , and the mode of motion, the added mass, M_H , and the wave-making damping coefficient, N_H , will be assumed to be given by

$$M_H = \frac{1}{2} \pi \rho \bar{y}^2 \quad \text{for both rigid-body-motion and vibration modes,} \quad (29)$$

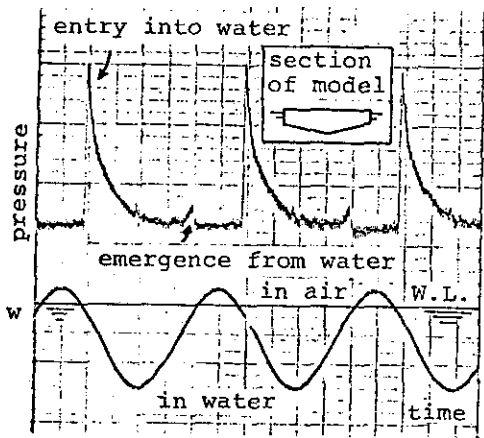


Fig. 5 Bottom pressure of a wedge-shaped model ship in oscillation test.

$$N_H = \begin{cases} \frac{\rho g^2}{\omega_e^3} [2 \sin(\kappa \bar{y}) \exp(-\kappa \bar{z})] & \text{for rigid-body-motion mode, (30)} \\ 0 & \text{for vibration mode,} \end{cases}$$

where κ is the wave number of the incident wave. By virtue of (30), the terms C^*_{rv} and C^*_{vv} can be disregarded.

For a ship section in air, external forces other than the weight are not taken into account.

A ship encountering a wave train may be subjected to slamming successively. To eliminate whipping vibrations caused by the previous slamming, unrealistically large structural damping will be introduced before a certain instant, which causes the ship to response to slams only after the instant.

NUMERICAL RESULTS FOR A DAMAGED SHIP

Principal dimensions of the damaged ship are as follows;

$$L \times B \times D \times d_{full} = 48.0 \times 8.5 \times 4.2 \times 3.9 \text{ m.}$$

The ship's midship section and body plan are shown in Figs. 6 and 7. When the damage occurred, she was advancing with speed $U = 9$ knots in seas of state 6 with fore- and aft-draft given by

$$d_f = 1.15 \text{ m}, \quad d_a = 2.65 \text{ m.}$$

Her weight distribution is given by Fig. 8. Slamming may occur when the encounter frequency, ω_e , is almost the same as those for heave and pitch, or when the wave length, λ , is around $1.4L (=67.2 \text{ m})$. It was reported by the captain that the wave height was 4 m. In this paper, the significant wave height is assumed to be given by Nippon Kaiji Kyokai's standard value $0.6 \sqrt{\lambda} (=4.92 \text{ m})$, which is in con-

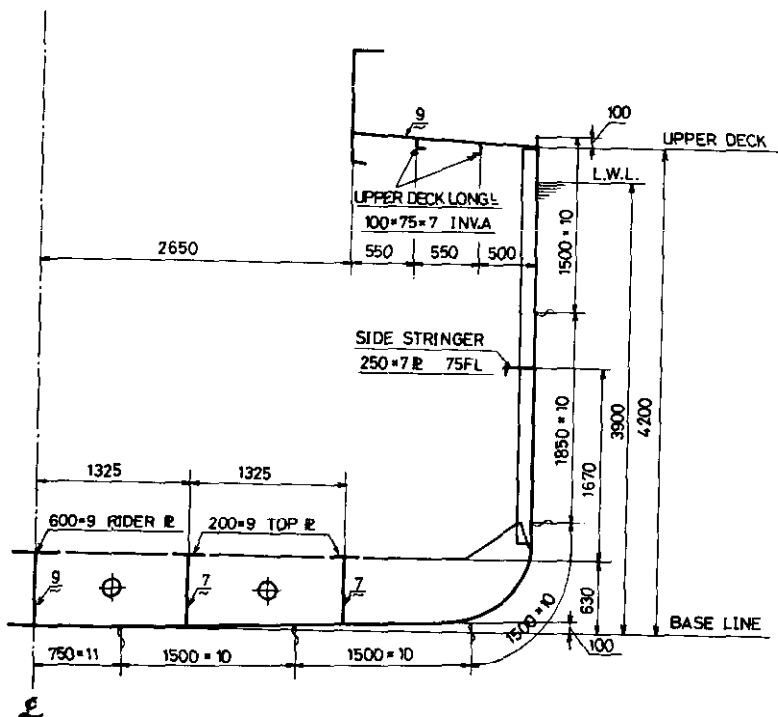


Fig. 6 Midship section of the damaged ship

formity with the captain's report, because his observed wave height 4m may be less than the actual one in the case of small ships. As can be seen in Fig. 7, the damaged section (S.S. 7) is almost the same as the midship section. The moment of inertia of the midship section, I , is given by

$$I = 606,136 \text{ mm}^2 \text{ m}^2,$$

and it will be assumed that the moment of inertia of each section is in proportion to the breadth of the section on load water line. The web area of section, A_w , is assumed to be constant;

$$A_w = 8,000 \text{ mm}^2.$$

The ultimate collapsing hogging moment of the damaged section, M_u , is obtained in Appendix 2, and is given by

$$M_u = 41.5 \text{ MNm}.$$

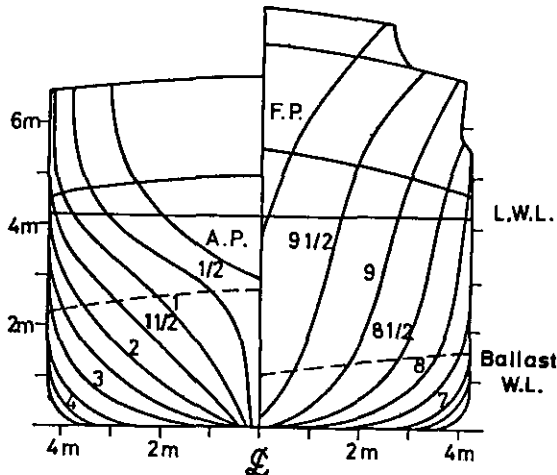


Fig. 7 Body plan

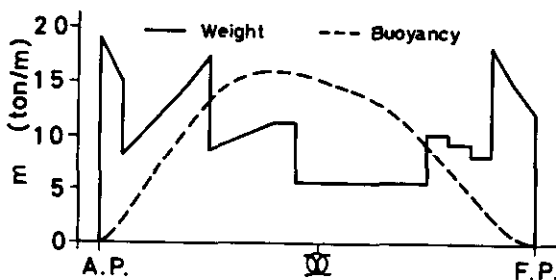


Fig. 8 Weight and buoyancy distributions

For the sake of simplicity, it will be assumed first that the ship encounters a regular wave train. Let H_w , ω , and κ be the wave height, the frequency, and the wave number, of the wave train, respectively. Results obtained are shown in Figs. 9 and 10 in which the same numerals encircled indicate an instant common to these figures. They show that the maximum hogging moment is lower than the ultimate collapsing moment, M_u . This situation is caused by the fact that the slamming impact travels forward from near the midship first, and after a certain time interval another impact travels aftward from her fore end. A considerable part of the hogging moment caused by the former is cancelled by the latter. Calculated bending moment results for the various wave heights are shown in Fig. 11. It is shown that the calculated peak hogging moments at S.S. 7 in regular waves never attain the ultimate collapsing moment even in unrealistically high waves; therefore, the damage could not occur in regular waves.

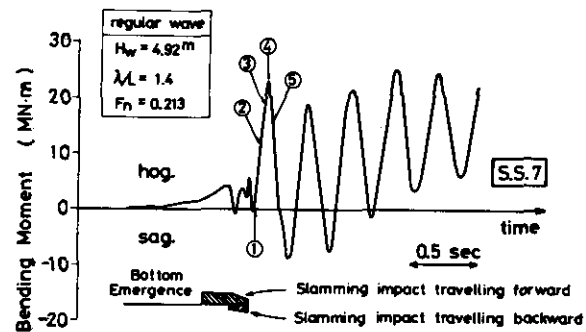


Fig. 9 Time history of bending moment at S.S. 7 in regular waves

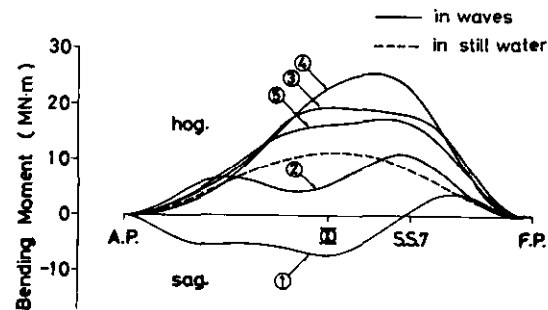


Fig. 10 Longitudinal bending moment distribution

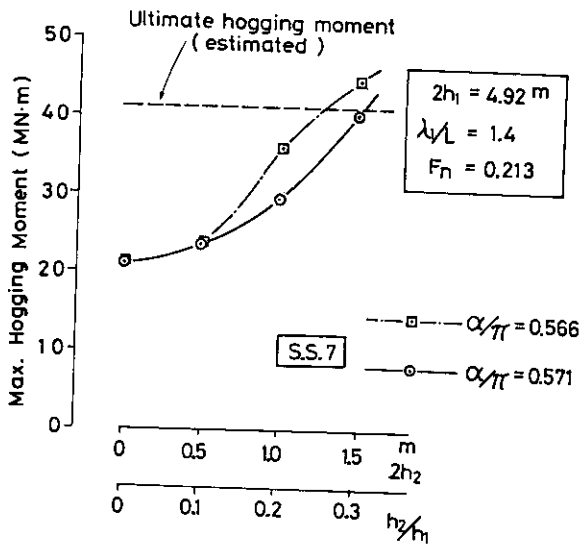


Fig. 11 Maximum hogging moment vs. wave height

Actual rough seas are not regular, but have a stochastic structure. Corresponding to the spectrum given by Fig. 12, the wave is assumed to be given in the two-term expression for ζ such that

$$\zeta = h_1 \cos(\kappa_1 X + \omega_1 t) + h_2 \cos[(2\kappa_1 X + \sqrt{2}\omega_1 t) + \alpha], \quad (31)$$

where

$$\kappa_1 = 2\pi/\lambda_1, \quad \lambda_1/L = 1.4, \quad \omega_1 = \sqrt{\kappa_1 g},$$

$$2h_1 = 4.92 \text{ m}, \quad 2h_2 = 1.48 \text{ m}.$$

Here α is defined by the phase angle at the instant when the ship's midship section crosses the crest line of the longer wave component of wave height $2h_1$ just before the occurrence of a slam; $\alpha/\pi = 0.566$ has been used as the standard value for the present calculations.

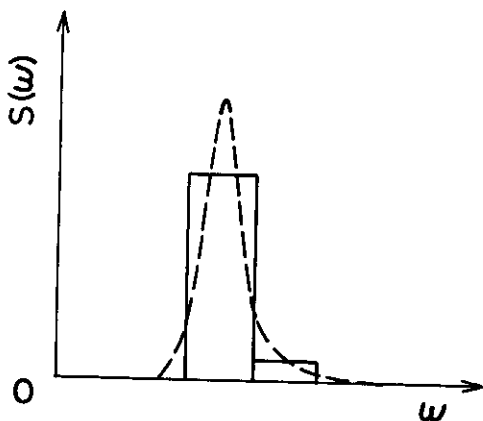


Fig. 12 Wave spectrum for an irregular wave

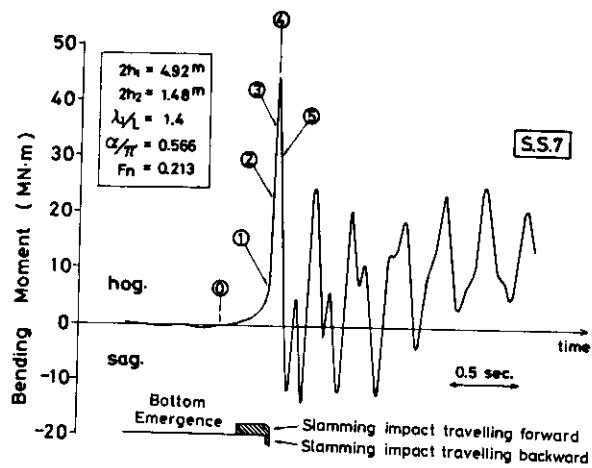


Fig. 13 Time history of bending moment at S.S. 7 in waves given by (31)

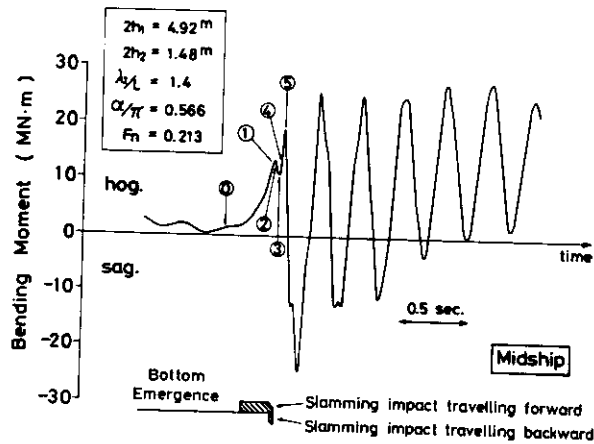


Fig. 14 Time history of bending moment at midship

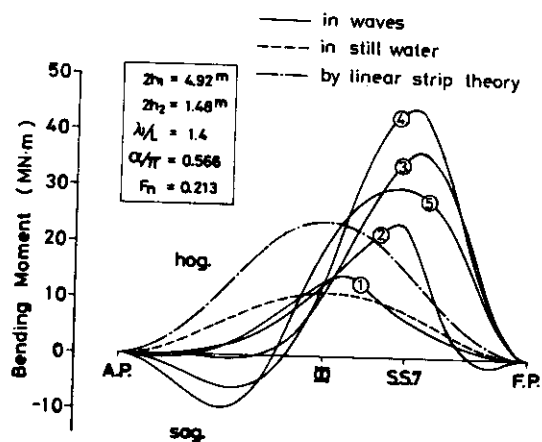


Fig. 15 Longitudinal bending moment distribution

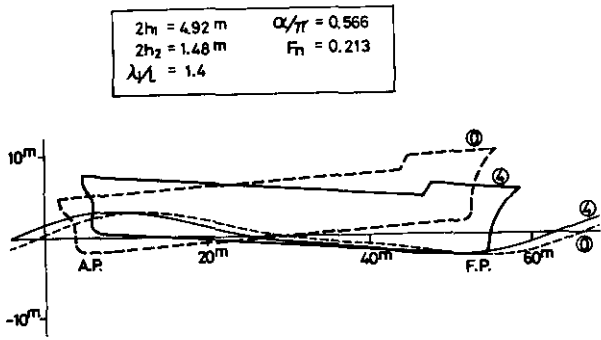


Fig. 16 Motion of ship relative to waves

In this sea condition, the ship's slamming impact travels forward from the mid-ship for a sufficiently long time interval before a bottom slam occurs in the fore end. The ship's bending moments obtained are shown in Figs. 13-15, its configurations are shown in Fig. 16, and behaviors of the slams are shown in Fig. 17. The points or curves with the same numerals encircled correspond to each other. Figs. 13 and 14 show the time history of bending moment at S.S. 7 and midship, and Fig. 15 shows their longitudinal distributions. As can be seen in Fig. 16, the wave profile is flat around S.S. 6 - S.S. 7 at the instant corresponding to ④, and at this moment significant slamming occurs around S.S. 7 causing a large hogging moment there of up to $M_{U1} = 41.5 \text{ MN}\cdot\text{m}$, which suggests the possibility of the occurrence of the damages at S.S. 7. Fig. 17 indicates that the bottom impact force takes a peak value at S.S. 7 earlier than the hogging moment.

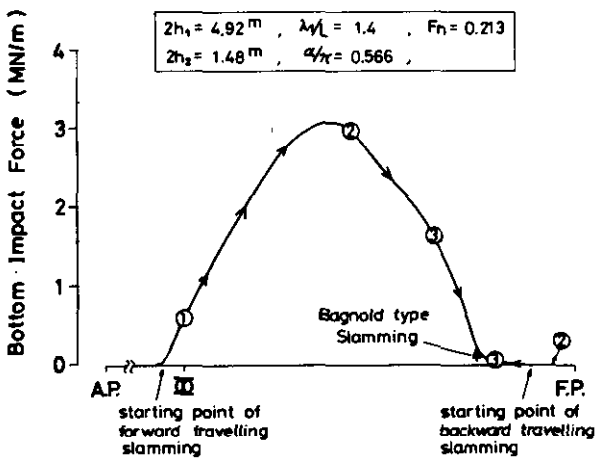


Fig. 17 Travel of bottom impacts

Effects of the phase difference, α , and the wave height, $2h_2$, of the shorter wave component are shown in Figs. 18 and 19. The decrease of the phase angle results in a complicated ship-wave configuration at the moment of slam, and the dotted line in Fig. 18 indicates estimates for the maximum hogging moment at S.S. 7, which are obtained by disregarding minor effects of slamming. Fig. 19 shows that the peak value of the hogging moment increases beyond the ultimate collapsing moment, M_{U1} , with the wave height, $2h_2$, of the shorter wave component. These results suggest that the ship's section under consideration could be collapsed by a high bending moment due to a slamming impact.

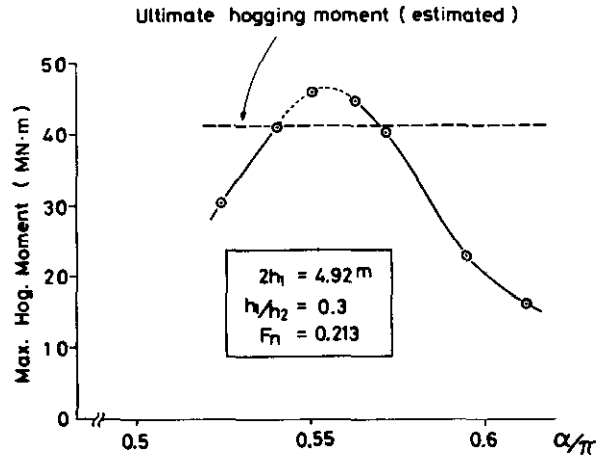


Fig. 18 Effects of phase difference of component waves on the maximum hogging moment at S.S. 7

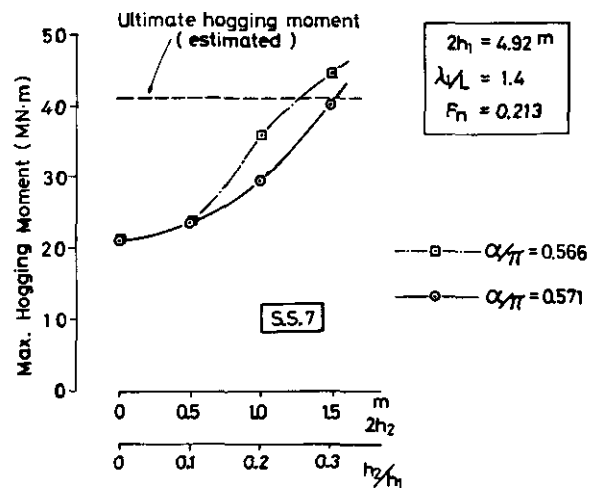


Fig. 19 Effects of height of the shorter wave component on the maximum hogging moment at S.S. 7

CONCLUSIONS

Structural damages of a single-bottomed small cargo ship due to slamming are analyzed with the aid of the finite element method by idealizing the ship's hull as a Timoshenko beam. Conclusions obtained are as follows:

- 1° Small cargo ships usually have a large trim in ballast conditions and often encounter relatively high waves compared with their dimensions. Among rough seas, more than half of the bottom may emerge from the water surface, and may be subjected to serious slamming impacts. Since the ballast water in the fore-peak tank works as a concentrated inertia, high hogging moment occurs around S.S. 7 due to its inertia force just after the instant of serious bottom slamming.
- 2° Bottom corrugations, which may be caused by previous slams, reduce the ultimate strength of the bottom plates and accordingly the effective section modulus for hogging. Therefore, the ultimate collapsing strength against hogging at the damaged section is reduced to about half that of the original design.
- 3° In regular waves, hogging moments caused by a slamming impact may be cancelled by a sagging moment caused by another, and therefore, large hogging moments do not occur. In irregular waves, however, the hogging moment becomes significantly large; the small cargo ship considered in this paper might suffer from structural damages due to high hogging moment caused by slamming among irregular waves.
- 4° To avoid this kind of damage, it is recommended that the fore-draft be increased. Double-bottomed structure is also effective for this purpose, because it increases the ultimate collapsing strength after bottom corrugation is generated.
- 5° The method used in this analysis, in which the ship's hull is treated as an assemblage of Timoshenko beam elements, is effective for the analysis of the behavior of the ship whose shear deflection or higher harmonic vibration cannot be disregarded.

ACKNOWLEDGMENTS

The authors wish to express their gratitude to Professor J. Fukuda, Kyushu University, and Professors H. Harada and M. Kawakami, Hiroshima University, for their instructive advice. The present investigation was supported by a grant-in-aid for scientific research from Ministry of Education, Japan.

REFERENCES

1. J. McCallum, "The strength of fast cargo ships," Trans. RINA, 1975.
2. J. D. Clarke, Discussion to committee report on derived loads, in Proc. 7th ISSC, Vol. 2, IRCN, Paris, 1979.
3. M. Kawakami and H. Muramoto, "On the damage of bottoms of small ships due to slamming," J. West-Japan Soc. N. A., Vol. 33, 1967. (in Japanese)
4. V. G. Szebehely and M. A. Todd, "Ship slamming in head seas," NSRDC Report 913, 1955.
5. V. G. Szebehely, "On slamming," NSRDC Report 995, 1956.
6. P. Kaplan, T. P. Sargent, and J. Cilmi, "Theoretical estimates of wave loads on the SL-7 container ship in regular and irregular seas," SSC, US Coast Guard, SSC-246(SL-7-4), 1974.
7. R. E. D. Bishop, W. G. Price, and P. K. Y. Tam, "On the dynamics of slamming," Trans. RINA, Vol. 120, 1978.
8. R. E. D. Bishop and W. G. Price, Hydroelasticity of Ships, Cambridge Univ. Press, 1979.
9. W. K. Meyerhoff and G. Schlachter, "Ein Ansatz zur Bestimmung der Belastung von Schiffen im Seegang unter Berücksichtigung hydrodynamischer Stösse," Jb. STG, Bd. 71, 1977.
10. Y. Yamamoto, M. Fujino, and T. Fukasawa, "Motion and longitudinal strength of a ship in head sea and the effects of nonlinearities," J. Soc. NA of Japan, Vols. 143 & 144, 1978, Vol. 145, 1979, (in Japanese); Naval Architecture and Ocean Engineering, Vol. 18, Soc. NA of Japan, 1980.
11. Y. Yamamoto, M. Fujino, T. Fukasawa, and H. Ohtsubo, "Slamming and whipping of ships among rough seas," in Numerical Analysis of the Dynamics of Ship Structures, EUROMECH 122, ATMA, Paris, 1979.
12. Y. Yamamoto, "Structure-fluid interaction problems for a ship among waves," Proc. 15th ICTAM, North-Holland, 1980.
13. Y. Yamamoto, "The Ritz procedure and its extensions in finite element analysis," in Computational Meth. in Nonlinear Mech., North-Holland, 1980.
14. T. Kumai, "Damping factors in the higher modes of ship vibration," European Shipbuilding, Vol. 7, 1958.

15. G. Aertssen and R. De Lembre, "A survey of vibration damping factors found from slamming experiments on four ships," Trans. N-ECIES, Vol. 87, 1970-71.
16. H. Ohtsubo, Y. Yamamoto, and Y.-J. Lee, "Ultimate compressive strength of wide rectangular plates," J. Soc. NA of Japan, Vol. 142, 1977. (in Japanese)
17. J. M. Murray, "Notes on deflected plating in compression and tension," Trans. INA, Vol. 87, 1945.

$$\xi = x - x_j,$$

$$l = x_{j+1} - x_j.$$

It can be confirmed that the difference, $w - w_s$, yields the flexural deflection, w_b . The rigid-body-motion mode of deflection, w_r , is expressed by

$$w_r = z_{\alpha} + (x - L/2) \theta$$

$$= [N_r] \{q_r\}, \quad (37)$$

where

$$[N_r] = [1, x] \begin{bmatrix} 1 & -L/2 \\ 0 & 1 \end{bmatrix}, \quad (38)$$

$$= [1, \xi, \xi^2, \xi^3] \begin{bmatrix} 1 & x_j - L/2 \\ 0 & 1 \\ 0 & 0 \\ 0 & 0 \end{bmatrix}, \quad (39)$$

$$\{q_r\} = \begin{Bmatrix} z_{\alpha} \\ \theta \end{Bmatrix}. \quad (40)$$

APPENDIX 1 TIMOSHENKO BEAM ELEMENT

Let x_j , $j = 1, \dots, N+1$, be the x -coordinates of nodal points of beam elements such that

$$x_1 = 0 \text{ and } x_{N+1} = L.$$

The total and shear deflections, w and w_s , can be expressed in each element by

$$w = [N_v]^j \{q_v^e\}^j, \quad (32)$$

$$w_s = [N_s]^j \{q_s^e\}^j, \quad (33)$$

where

$$[N_v]^j = [1, \xi, \xi^2, \xi^3] \times$$

$$\times \begin{bmatrix} 1 & 0 & 0 & 0 & 0 & 0 \\ 0 & -\frac{1}{l} & 1 & 0 & \frac{1}{l} & 0 \\ -\frac{3}{l^2} & \frac{3}{l^2} & -\frac{2}{l} & \frac{3}{l^2} & -\frac{3}{l^2} & -\frac{1}{l} \\ \frac{2}{l^3} & -\frac{2}{l^3} & \frac{1}{l^2} & -\frac{2}{l^3} & \frac{2}{l^3} & \frac{1}{l^2} \end{bmatrix}, \quad (34)$$

$$[N_s]^j = [1, \xi, \xi^2, \xi^3] \times$$

$$\times \begin{bmatrix} 0 & 1 & 0 & 0 & 0 & 0 \\ 0 & -\frac{1}{l} & 0 & 0 & \frac{1}{l} & 0 \\ 0 & 0 & 0 & 0 & 0 & 0 \\ 0 & 0 & 0 & 0 & 0 & 0 \end{bmatrix}, \quad (35)$$

$$\{q_v^e\}^j = \begin{Bmatrix} w_j \\ w_{sj} \\ \theta_{bj} \\ w_{j+1} \\ w_{sj+1} \\ \theta_{bj+1} \end{Bmatrix}, \quad (36)$$

Now the deflections are expressed in each element in the following form:

$$w = [N_v]^j \{q_v^e\}^j + [N_r] \{q_r\}, \quad (41)$$

$$w_s = [N_s]^j \{q_s^e\}^j, \quad (42)$$

$$w_b = [N_{vb}]^j \{q_v^e\}^j + [N_r] \{q_r\}, \quad (43)$$

where

$$[N_{vb}]^j = [N_v]^j - [N_s]^j,$$

$$\{q_v^e\}^j = \begin{Bmatrix} w_{vj} \\ w_{sj} \\ \theta_{bj} \\ w_{vj+1} \\ w_{sj+1} \\ \theta_{bj+1} \end{Bmatrix}. \quad (44)$$

Introducing (41) and (42) into (20) leads to the elementwise equation of motion, whose coefficient matrices and constant vector are given in the following form:

$$\begin{bmatrix} M_{rr}^e + M_{rr}^{*e} & M_{rv}^e + M_{rv}^{*e} \\ M_{vr}^e + M_{vr}^{*e} & M_{vv}^e + M_{vv}^{*e} \end{bmatrix}$$

$$= \int_0^L [N_r \ N_v]^j T \begin{bmatrix} m + M_H & 0 \\ 0 & m + M_H \end{bmatrix} [N_r \ N_v]^j d\xi ,$$

$$[K_{VV}^e] = \int_0^L EI [N_{vb}''']^j T [N_{vb}''']^j d\xi + \int_0^L GA_w [N_s']^j T [N_s']^j d\xi ,$$

$$[C_{VV}^e] = \frac{\delta z}{\pi \omega^2} [K_{VV}^e] ,$$

$$\begin{bmatrix} C_{rr}^* & C_{rv}^* \\ C_{vr}^* & C_{vv}^* \end{bmatrix}$$

$$= \int_0^L [N_r \ N_v]^j T \begin{bmatrix} N_H & 0 \\ 0 & N_H \end{bmatrix} [N_r \ N_v]^j d\xi ,$$

$$\begin{bmatrix} K_{rr}^* & K_{rv}^* \\ K_{vr}^* & K_{vv}^* \end{bmatrix}$$

$$= \int_0^L \rho g B^* [N_r \ N_v]^j T [N_r \ N_v]^j d\xi ,$$

$$\begin{Bmatrix} \hat{r}^* \\ \hat{v}^* \end{Bmatrix} = \int_0^L [N_r \ N_v]^j T \{ (-\dot{w} + U_w' + v_z) \dot{M}_H$$

$$+ (U_w' + \dot{v}_z) M_H + (U_w' + v_z) N_H$$

$$+ \rho g (A - B^* w) - mg \} d\xi ,$$

where prime indicates differentiation with respect to x or ξ , and B^* is the breadth of water line in each section in still water condition. The total matrices and vector can be obtained by assembling those obtained elementwise.

In the present computations, the number of elements for the ship girder is taken as $N=20$ which corresponds to $\Delta x = L/20$, and the discrete time interval, Δt , is determined by taking account of the natural period of elements such that $\Delta t = 0.0005$ sec.

APPENDIX 2 ULTIMATE COLLAPSING MOMENT

The ultimate collapsing moment of the ship at S.S. 7 in the hogging condition will be considered herein. According to the report, the ship's bottom and side shell structure were seriously buckled, which may result in a significant decrease of their structural efficiency. Presumably the side shell was buckled after the bottom. As can be seen in the midship section shown in Fig. 6, the middle part of the ship is single-bottom-

ed with transversely stiffened plating of 10-11 mm in thickness, and her section at S.S. 7 is almost the same as at the midship section (see Fig. 7). According to the inspection data of a sister ship, the bottom plating has been corrugated up to 18 mm over a wide range, which may possibly be caused by previous bottom slamming as can be expected from Kawakami and Muramoto's investigation [3]. In the following, the initial deflections in the bottom plating of the ship under consideration will be assumed to be two times the thickness. The efficiency of the bottom plating may thereby be decreased to a certain extent, and this situation will be investigated on the basis of experiments.

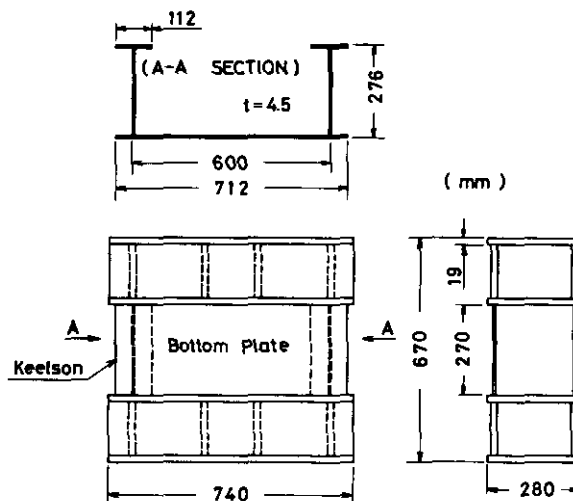


Fig. 20 Test model



Photo 1 Collapsed model B

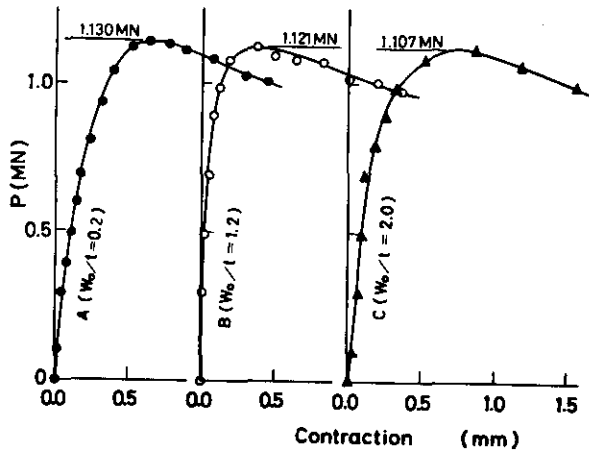


Fig. 21 Test results for compressive load vs. contraction

The models of the single bottom structure are as shown in Fig. 20. The initial deflections were formed by press beforehand for Models B and C. The model was compressed longitudinally under a testing machine. Photo 1 shows one of the models (Model B) after the collapsing test. Fig. 21 shows test results for the compressive load versus contraction curves, and the ultimate collapsing load decreases slightly with the increase of the initial deflections, which are investigated from the theoretical point of view [16, 17].

Consider a simply supported rectangular plate, ($a \times b \times t$), as shown in Fig. 22. The formulas can be derived by assuming that initial and addition deflections are expressed in the form

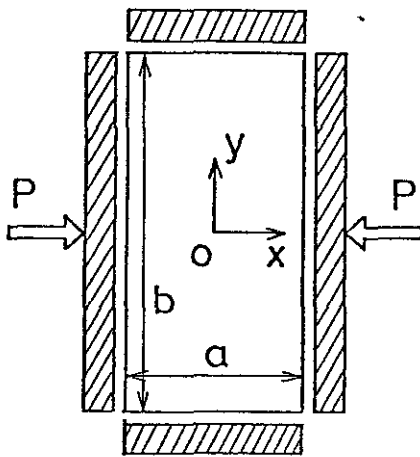


Fig. 22 Simply supported rectangular plate

$$w_0 = W_0 \cdot \cos(\pi x/a) \cos(\pi y/b), \quad (51)$$

$$w = W \cdot \cos(\pi x/a) \cos(\pi y/b). \quad (52)$$

Introducing these expressions into the von Karman equation modified by taking account of initial deflections leads to the formula for the mean compressive stress, p , given by

$$\frac{p}{P_E} = \frac{W}{W+W_0} + \frac{P_1}{P_E t^2} (W^2 + 2W W_0), \quad (53)$$

The average edge compressive strain, e , becomes as

$$e = \frac{p}{E} + \frac{P_0}{E t^2} (W^2 + 2W W_0). \quad (54)$$

Thus the efficiency of plating, η , is defined by

$$\eta = \frac{b e}{b} = \frac{p}{E e}. \quad (55)$$

Here b_e is the effective breadth, P_E is the buckling stress of the plate; P_E , P_0 , and P_1 are given by

$$P_E = \left(1 + \frac{a^2}{b^2}\right) \frac{\pi^2 E}{12(1-\nu^2)} \frac{t^2}{a^2},$$

$$P_0 = \frac{\pi^2 E}{8} \frac{t^2}{a^2},$$

$$P_1 = \left(1 + \frac{a^4}{b^4}\right) \frac{\pi^2 E}{16} \frac{t^2}{a^2}.$$

The effective breadth, b_e , of a rectangular plate depends largely upon the initial and additional deflections,

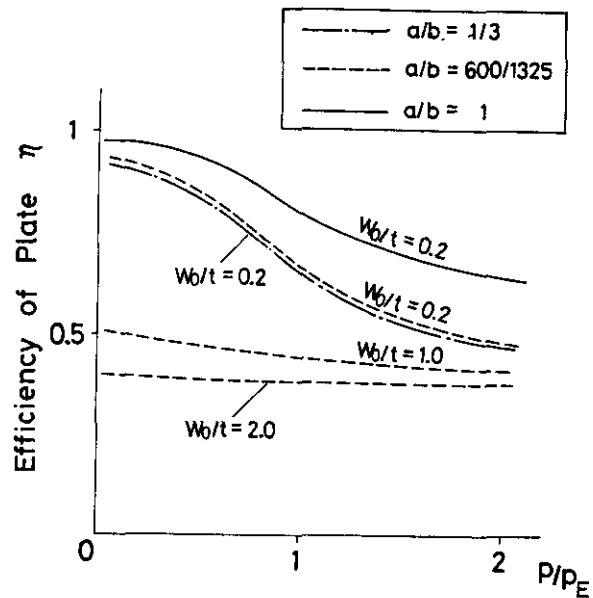


Fig. 23 Reduction of in-plane efficiency η due to corrugation

W_0 and W , and it is obtained in the following form after Murray's consideration [17]: (see Fig. 23)

$$\eta = \frac{be}{b} = 1/[1 + \frac{P_0}{P_1}(1 - \frac{PE}{P} \frac{W}{W+W_0})] \quad (56)$$

In the case of sufficiently large W_0/t , η may be approximated by

$$\eta \approx \eta_{\infty} = 1/(1 + p_0/p_1) \\ = 1/[1 + 2/(1 + a^*/b^*)] \quad (57)$$

The bottom plating is stiffened longitudinally and transversely with spacing 1,325 mm (= b) or 600 mm (= a), and therefore, η_{∞} equals 0.343. Namely, the in-plane rigidity of the deflected bottom plate is reduced to almost one third that of the flat plate.

In order to estimate the ultimate compressive strength, P_u , of the plate, it is assumed, according to von Karman, that the mean compressive stress attains its maximum value P_u when the compressive stress along the edges $y = \pm b/2$ arrives at a fraction of yield stress, $c\sigma_y$, where σ_y is the yield stress of materials and c is a correction factor to be determined by the help of experiments. Now the following formula is obtained:

$$P_u = \eta c \sigma_y b t, \quad (58)$$

where η is a function of P_u/bt . By virtue of (55), it is evident that the maximum compressive load is calculated by multiplying the effective sectional area of the plate, $\eta \cdot bt$, by a fraction of yield stress, $c\sigma_y$. The ultimate compressive strength can easily be estimated for a thin walled structure. In the case where stiffeners are rather weak, $c\sigma_y$ can be regarded as the lateral buckling stress of the stiffeners. The ultimate collapsing load for a thin walled structure is estimated by

$$P_u = c\sigma_y \Sigma \eta A, \quad (59)$$

where A is the sectional area of component plate, and the summation is taken over all the components.

This procedure can be applied for estimating the ultimate load of the test models. The measured maximum initial deflections are as follows;

$$W_0/t = 0.2 \text{ (Model A), } 1.2 \text{ (Model B),}$$

$$2.0 \text{ (Model C) for bottom,}$$

$$W_0/t = 0.2 \text{ (Models A, B and C)}$$

for girders.

As for the flange plate, it is assumed

to have no initial deflections. By using $\sigma_y = 287 \text{ N/mm}$ obtained by tests, the ultimate load, P_u , of a model can be determined with the use of (59). Assuming that $c = 0.83$, it is given by

$$P_u = 1.19(A), 1.11(B), 1.08(C) \text{ MN,}$$

which corresponds to that obtained by experiments

$$P_u = 1.13(A), 1.12(B), 1.11(C) \text{ MN.}$$

In this case, $c\sigma_y$ may be regarded as the buckling stress of the flange plate by crippling (see Photo 1). The collapsing moment of a thin walled structure can also be calculated by

$$M_u = c\sigma_y Z_u, \quad (60)$$

where Z_u is the section modulus obtained by the use of the effective sectional area of plate components.

The ultimate collapsing moment, M_u , of the actual ship can be estimated: Assuming the initial deflections of the bottom plates are more than two times the thickness, η becomes 0.35. For the bottom girder and side shell under compression, the initial deflection of $W_0/t = 0.2$ was used for the calculation. The flange plates were assumed to have no initial deflections. Now the effective section modulus becomes as follows;

$$Z_u = 212,500 \text{ mm}^2 \text{ m,}$$

which is some 50% of the designed value, $Z = 412,600 \text{ mm m}$. Correspondingly, the height of the neutral axis above the base line raises significantly from 1,607 mm to 2,065 mm. Now the ultimate collapsing moment can be obtained by the use of $\sigma_y = 235 \text{ N/mm}$ and $c = 0.83$ derived from the compression tests;

$$M_u = 41.5 \text{ MN m.}$$

The validity for adopting this c -value is asserted from the following fact: The ship had a deeper double bottom in the fore part of its long hold, and the damage occurred at the fore end of the regular single bottom structure; therefore, the flanges of keelsons in the damaged section were subjected to the additional compressive force due to local bending of the bottom structure.

Moreover, if the ship is double-bottomed, the effective sectional modulus may be influenced but slightly by bottom corrugation.